PHYSICAL REVIEW B VOLUME 53, NUMBER 8 15 FEBRUARY 1996-II

Thermal formation of Zn-dopant-vacancy defect complexes on InP(110) surfaces

Ph. Ebert, M. Heinrich, M. Simon, C. Domke, and K. Urban
Institut für Festkörperforschung, Forschungszentrum Jülich GmbH, D-52425 Jülich, Germany

C. K. Shih
University of Texas, Austin, Texas 78712

M. B. Webb and M. G. Lagally
University of Wisconsin, Madison, Wisconsin 53706
(Received 21 August 1995)

The thermal formation of Zn-dopant-vacancy defect complexes is studied as a function of annealing time and temperature between 293 and 480 K on InP(110) surfaces using scanning tunneling microscopy. The geometric and electronic structure as well as the concentrations of isolated dopant atoms, phosphorus monovacancies, and vacancy-Zn defect complexes are found to be related to each other. An attractive interaction between the vacancies and Zn atoms is found. The vacancies and Zn-dopant atoms can compensate each other's charge and form uncharged complexes. The formation of these compensated defect complexes strongly decreases the concentration of electrically active Zn atoms. The total observable Zn concentration in the surface layers remains constant with time at temperatures up to 415 K. Only defect complexes consisting of a surface vacancy and a subsurface dopant atom are formed. At 480 K the observable Zn concentration decreases, however, because defect complexes consisting of a *subsurface* vacancy and a Zn atom are formed.

I. INTRODUCTION

The achievement of high carrier concentrations in compound semiconductor crystals and multilayers is crucial for technological applications. Suitable smooth as well as abrupt changes of the concentration of electrically active dopants over atomic distances determine the electrical properties of semiconductor devices. For example, multilayer structures consisting of δ-doping profiles yield a particularly high mobility of charge carriers for high-speed applications. Such a spatial confinement of charge carriers in atomic structures, however, is to a large degree governed by the properties, energetics, and thermodynamics of the dopants and related defect-dopant complexes. For example, a charge repulsion in δ-doped GaAs multilayers[1] or the formation of compensating defect-dopant complexes[2] can considerably reduce the concentration of electrically active dopant atoms and thus limit possible applications. Similarly, the charge-carrier concentration on the surface is, on the one hand, increased by surface and near-surface dopant atoms and, on the other hand, may be reduced by compensating for native point defects formed on the surface, as we will show in this paper.

Scanning tunneling microscopy (STM) is particularly well suited for investigations of near-surface dopant atoms and their defect complexes, because STM makes it possible to identify individual atomic defects and explore their properties. In particular, III-V semiconductor surfaces with (110) orientation have a simple relaxation, and can be reproducibly obtained by cleavage lending themselves well to model studies of defects, such as antisite defects,[3] vacancies,[4–6] and dopant atoms.[7–11] Unlike thermally cleaned Si(001) surfaces, the cleaved III-V(110) surfaces have a very low density of defects [e.g., for our InP(110) surfaces the vacancy density is 2×10^{11} cm^{-2} directly after cleavage[12]], which makes these surfaces ideal for investigations of *isolated* defects. To our knowledge, most previous studies focused on *isolated* defects. Only recently has the charge of As vacancies on GaAs(110) been deduced from an observation of the compensation of the charge of vacancies by dopants.[13] Thus dopants and native defects, such as vacancies, may interact. Furthermore, it has been demonstrated that the vacancy concentration on InP(110) and GaAs(110) surfaces can be reproducibly changed over more than one order of magnitude by suitable annealing.[12] Thus these systems offer ideal conditions to explore the *interactions between defects* and the *formation of defect complexes* on the atomic scale.

In this paper we present an extensive investigation of Zn-dopant atoms and thermally formed Zn-vacancy defect complexes in InP(110) surfaces. We explore the concentration and structure of isolated dopant atoms and vacancy-dopant complexes as a function of the vacancy concentration, the annealing time of the samples, and the temperature. We will focus on the following results in detail.

(i) The structure and electronic properties of isolated Zn-dopant atoms on InP(110).

(ii) The interaction between vacancies and Zn-dopant atoms, resulting in the formation of vacancy-Zn complexes and dipoles with a gradual charge compensation.

(iii) At low temperatures this formation of vacancy-Zn dipoles and complexes is the origin of a decrease of the concentration of negatively charged Zn dopants. The actual concentration of observable Zn atoms in the surface layers remains, however, constant with time. Only defect complexes with a vacancy in the surface layer are formed.

(iv) Finally, the concentration of observable Zn atoms decreases drastically with time at 480 K. It is suggested that vacancy-Zn complexes are formed in the bulk.

 © 1996 The American Physical Society

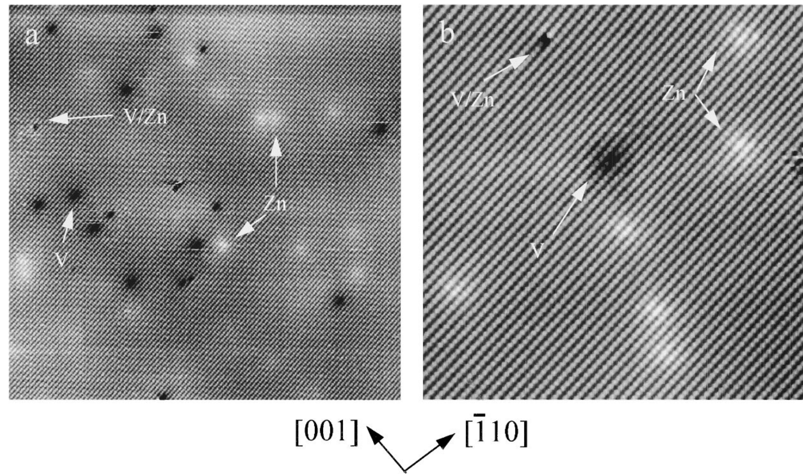

FIG. 1. Overview of the defects occurring on InP(110) surfaces. The images have been obtained with a STM after cleaving and annealing the surface for 5 min at 480 K. In the 75×75-nm^2 overview image (a), measured at a sample voltage of -2.4 V, three different types of defects are visible. These are phosphorus vacancies (marked *V*) appearing as black depressions, white elevations surounding Zn-dopant atoms Zn, and very localized black dots. The latter are vacancy-Zn-dopant complexes and are marked with *V*/Zn. One cleavage-induced vacancy cluster is also present in the upper left corner. Unlike the monovacancies the vacancy clusters are not thermally formed. (b) STM image with atomic resolution showing the three different types of defects. Six dopant atoms in different subsurface layers, one vacancy, and one vacancy-dopant complex are visible and marked as in (a). The scan width is 25×25 nm^2 (sample voltage -2.2 V).

II. EXPERIMENT

The experiments were performed with liquid-encapsulated Czochralski (LEC)-grown *p*-type InP single crystals, which had Zn concentrations of nominally $(1.3–2.1)\times10^{18}$ cm^{-3}.[14] The samples were cleaved in *ultrahigh vacuum* to form reproducibly clean (110) surfaces. After cleavage, the InP crystals were annealed *ex situ* to fixed temperatures between 293 and 480 K at a pressure of 5×10^{-9} Pa. The heating was performed for some time *t* before the samples were radiation cooled to room temperature within typically 30 min. The sample was then transferred to the beetle-type STM (Ref. 15) without breaking the vacuum, and investigated. The STM images were obtained in the constant-current mode. After each investigation with STM, the samples were reheated several times at the same fixed temperature to determine the time evolution of the defect concentrations. For each temperature an additional sample was cleaved. The temperature was measured with a thermocouple pressed against the sample holder, and calibrated by the melting points of In alloys soldered on the uncleaved sample. The temperature uncertainty is estimated to be ±10 K. We used electrochemically etched tungsten tips conditioned *ex situ* by field emission.

III. STRUCTURE OF ISOLATED DOPANT ATOMS

Figure 1(a) is a typical large-scale STM overview of the InP(110) surface showing several defects. Three types of defects can be distinguished by their contrast. The first defect type appears as apparent elevations (marked Zn), while the second defect is surrounded by apparent black depressions (*V*). A few defects are more difficult to see, since they are neither surrounded by elevations nor depressions (*V*/Zn). They are only recognizable as an atomically localized hole. In Fig. 1(b) these three different types of defects are shown at a higher magnification. The dark depressions (marked *V*) are surrounding isolated positively charged phosphorus monovacancies, whose structure has previously been analyzed in detail elsewhere.[4,6,16] The white elevations (marked Zn) are due to isolated negatively charged Zn_{In} dopant atoms. We will discuss their properties in this section. The third type of defects appears as one missing dangling bond (marked *V*/Zn) adjacent to a bright dangling bond. These defects are defect complexes consisting of a vacancy and an adjacent Zn dopant atom. A discussion of these complexes and of the interaction between dopants and vacancies is presented in Sec. IV. The three types of defects visible in Fig. 1 account for almost all defects on the surface. In addition we observed a few adatoms[17] and, rarely, defects which might be associated with subsurface vacancies. Some cleavage-induced vacancy clusters were also present, but their density is negligible compared to that of the three defect types discussed in this paper.

A. Discussion of the nature of the defects (marked Zn)

We mentioned above that defects appearing as wide elevations are Zn_{In} dopant atoms. Their nature has been previously discussed for similar defects on GaAs(110) surfaces.[7,9] However, we will briefly present the arguments leading to the conclusion that the Zn-marked defects are in fact Zn-dopant atoms.

(i) Contaminations of the sample can be excluded because the defects can be observed directly after cleavage, and their density does not increase with time.

(ii) Crystal impurities other than dopant atoms have a maximum density below 10^{16} cm^{-3}. The defects observed here have densities of about $(2–3)\times10^{18}$ cm^{-3}, hence they cannot be impurities.

(iii) Phosphorus vacancies can also be ruled out, because they have a different appearance and structure, and are not expected to be negatively charge on *p*-type surfaces. Furthermore the anion vacancies are formed thermally with a strong

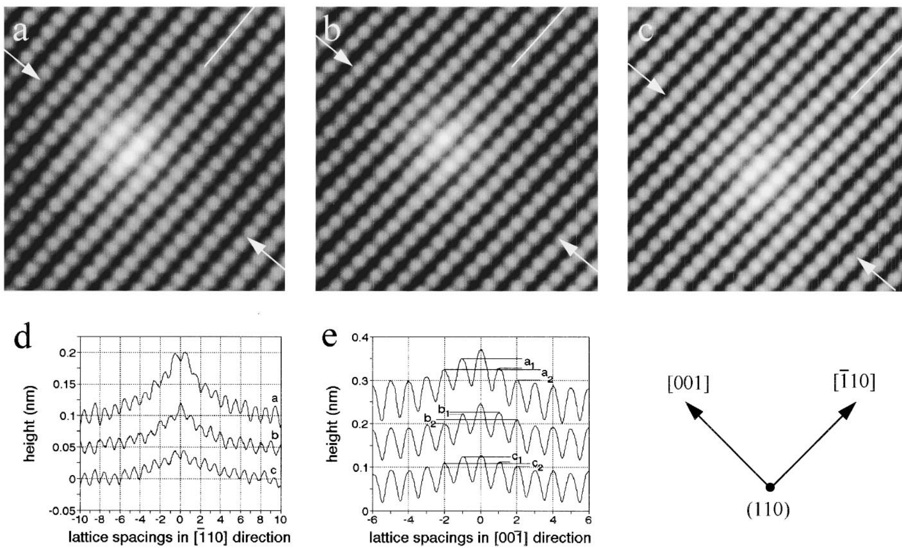

FIG. 2. Zn-dopant atoms of type *a* in the first (a), type *b* in the second (b), and type *c* in the third (c) subsurface layer. The arrows indicate the mirror plane of the defects. (d) and (e) show the height profiles (labeled *a*, *b*, and *c*) in $[\bar{1}10]$ and $[00\bar{1}]$ directions through the respective defects visible in (a), (b), and (c). The profiles show the symmetry of the defects.

temperature dependence,[12,17] unlike the defects observed as bright elevations. The anion vacancies have been described previously for InP(110),[6] GaP(110),[4] and GaAs(110) (Refs. 5 and 18) surfaces, and appear in Fig. 1 as black depressions.

(iv) Indium vacancies essentially do not occur on our *p*-type samples.[12,17] In addition, they would not be expected to be negatively charged. The few missing In atoms observed were always touching vacancy clusters. Furthermore, cation vacancies seem to exist preferentially in notable concentrations on *n*-doped surfaces.[5]

(v) Adatoms can be observed occasionally on the InP(110) surfaces.[4,17] They are, however, uncharged, and are very localized features without the large charge-induced band-bending area surrounding them. Furthermore they are very mobile, unlike the defects observed here. Thus they are not identical to the defects studied here.

(vi) Antisite defects P_{In} cannot explain our observations either, because they are expected to be uncharged or positively charged on *p*-doped surfaces. They were investigated on GaAs(110),[3] and showed a distinctly different contrast. In addition, the In_P antisite defect cannot explain our defects either, because our material investigated was slightly phosphorus rich. In such a material In_P antisite defects do not occur in sufficient concentrations to explain the density of defects.

The only type of defect which can be correlated with the negatively charged defects observed are Zn-dopant atoms. They are expected to be negatively charged, because they are shallow acceptors of electrons. In addition, the observed defect concentration agrees with the dopant concentration of the crystals. On GaAs(110) it has been shown that the density of these defects follows exactly the concentration changes of superlattices[1,19] and doping profiles.[9] All this suggests that the defects marked Zn in Fig. 1 are indeed Zn-dopant atoms. More evidence will appear during the detailed analysis of the data.

B. Appearance of isolated Zn-dopant atoms on InP(110)

The STM images of the Zn-dopant atoms reveal several different symmetries and apparent height changes of the surrounding P sublattice similar to Be and Zn dopants on GaAs(110) surfaces.[7] These observations will lead to the conclusion that STM probes Zn-dopant atoms in several subsurface layers. Furthermore, the measurements show that the Zn atoms are in fact on substitutional In lattice sites.

Figure 2 shows three different Zn-dopant atoms obtained at -1.1 V tunneling voltage. All three defects have a $(00\bar{1})$ mirror plane (indicated by two arrows in each image). The mirror plane is either localized between the atomic rows along the [001] direction [Figs. 2(a) and 2(c)] or on top of the atomic rows [Fig. 2(b)]. The locations of the mirror planes relative to the atomic rows are also visible in the respective height profiles [Fig. 2(d)] in the $[1\bar{1}0]$ direction. The line cuts labeled *a*, *b*, and *c* in Fig. 2(d) [obtained from the Zn-dopant atoms imaged in Figs. 2(a), 2(b), and 2(c), respectively] show the corrugation through the center of the defect along the atomic rows marked by the dashed lines. The symmetry shows up in an equal raising of two atoms (a,c) or only one atom (b). Thus the center of the defect is located either in between or underneath the atomic rows in the [001] direction.

In contrast, there is no mirror plane with a $(\bar{1}10)$ orientation. The atoms on one side of the defects' maximum appear brighter than those on the other side. This is clearly visible in the height profiles along the [001] direction in Fig. 2(e). In the height profiles *a* and *c* the first and second atoms to the left side of the maximum (atoms at -1 and -2 lattice spacings) are more raised than the respective atoms on the right side ($+1$ and $+2$ lattice spacings). This is just reversed for profile *b*. Thus the centers of defects *a* and *c* are shifted toward the [001] direction, while that of defect *b* is displaced in the $[00\bar{1}]$ direction relative to the atomic rows in the $[\bar{1}10]$ direction.

Finally Figs. 2(d) and 2(e) show that the magnitude of apparent height changes of the underlying P sublattice decreases from defect *a* to defect *c*. At the specific sample voltage of Fig. 2 (-1.1 V) the highest elevation relative to the defect-free P sublattice of defects *a*, *b*, and *c* reaches about 0.09, 0.06, and 0.04 nm, respectively.

This apparent rise is also strongly dependent on the tunneling voltage, but the relative order of magnitude of the height change does not change. Defect *a* always appears

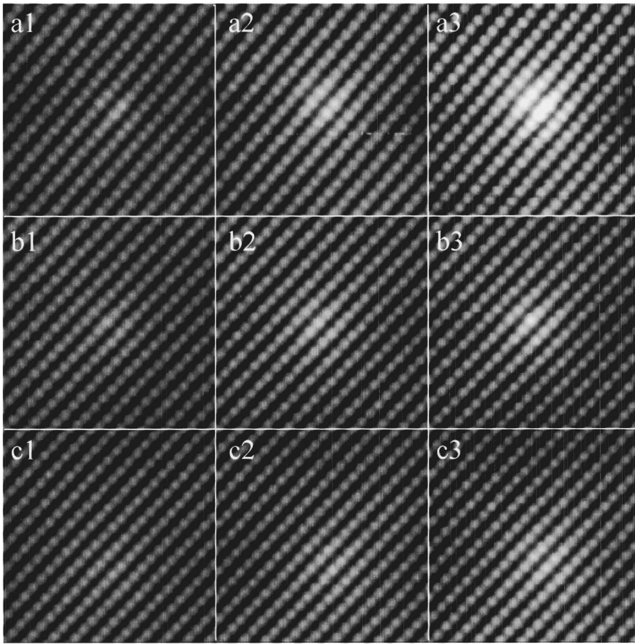

FIG. 3. Voltage dependence of the contrast of Zn-dopant atoms of type a (in the surface layer) ($a1-a3$), type b (second layer) ($b1-b3$), and type c ($c1-c3$) (third subsurface layer). The white-to-black corrugation change is about 0.9 nm for image ($a3$), and the values of the gray scale are comparable for all images. The figures labeled with an additional 1, 2, and 3 have been measured at -2.4, -1.5, and -1.1 V, respectively, with the exception of ($c1$), which has been measured at -1.8 V. The images have the same orientation as those in Figs. 1 and 2.

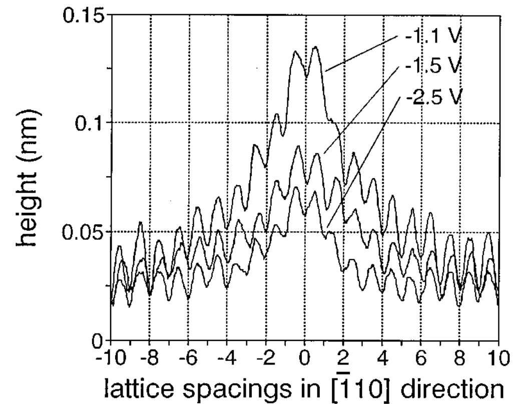

FIG. 4. Height profiles through a Zn-dopant atom of type a (in the first layer) at different voltages. The profiles were measured along the [$\bar{1}$10] direction.

more raised than defect b or c. It should be noted that the brightest defect has always the (1$\bar{1}$0) mirror plane between two [001] rows (two atoms are equally raised).

The voltage dependence of the Zn-dopant atoms is summarized in Fig. 3. All images in Fig. 3 have been measured and treated in exactly the same way, such that the values of the gray scale are comparable. The figure sets labeled a, b, and c are the dopant atoms of Figs. 2(a), 2(b), and 2(c), respectively. The figures labeled with an additional 1, 2, and 3 have been measured at -2.4, -1.5, and -1.1 V, respectively. The figure labeled $c1$ was measured at -1.8 V, because at higher negative voltages the defect was not visible. The brightest Zn atom is in the upper right corner, while in the lower left corner nearly no visible elevation remains. Figure 4 shows the effect of the voltage on the height profiles of the brightest Zn-dopant atom, which is situated in the first layer, as will be discussed below.

The charge of the dopant atoms is screened with a screening length of about 1.2 nm. It has been deduced using the procedure previously applied to defects on Si (Ref. 20) and vacancies on III-V semiconductors.[21,22] This procedure is based on the assumption that the charge-induced band bending yields a height change proportional to the screening factor $\exp(-r/R_s)$. The value of the screening length is in good agreement with the screening length determined for the P vacancies on the same surface.[23]

C. Structural model of the different Zn-dopant atoms

The apparent elevations surrounding every Zn-dopant atom are due to a charge-carrier accumulation around the negatively charged dopants. This accumulation induces an upward band bending which is visible in the STM images.[20,21] The voltage dependence of this charge accumulation in the STM images is typical of charged defects and has been previously observed and discussed for P and As vacancies[4,17] and dopant atoms.[7,10,11] In order to understand the voltage-dependent contrast, it is necessary to take both the charge accumulation around the Zn-dopant atoms and the tip-induced band bending into account. Each Zn is surrounded by a cloud of holes which screen the negative charge. The negative sample voltage induces an additional accumulation of electrons, creating a downward band bending. This tip-induced band bending follows the tip and thus affects the surface similarly at all locations. The charge cloud around the dopant atom is, however, localized and subsequently leaves an elevation in the STM images. The relative current extracted from the additional states available for tunneling due to the charge-induced upward band bending changes with the voltage. At larger negative voltages more states contribute to the tunneling current, and thus the relative effect of the Zn-induced upward band bending decreases. This is reflected in the STM images, which show a decrease of the brightness of the dopant atoms with increasing absolute value of the voltage (Figs. 3 and 4).

The largest band bending of the Zn-dopant atom is expected to occur directly at the site of the Zn atom itself. Thus the center of the elevation visible in STM images should reveal the lateral position of the charge and thus of the Zn atom itself. In addition, the symmetry and brightness reflects the depth of the Zn atom. The defects in Fig. 2 have the center of the band bending located either between two atomic rows in the [001] direction, slightly displaced in the [001] direction, or on top of a [001]-oriented row and displaced in the [00$\bar{1}$] direction. These locations alternate with decreasing magnitude of the apparent elevation of the defects. This can be directly correlated with different surface and subsurface positions of the Zn atom. First we consider substitutionally incorporated Zn_{In} atoms. Figures 5(a) and 5(b) show top and side views of Zn atoms incorporated in the first, second, and third layers. The Zn atom in the first layer has two nearest-neighbor P atoms in the surface, which are expected to be equally bright in the STM images. These two

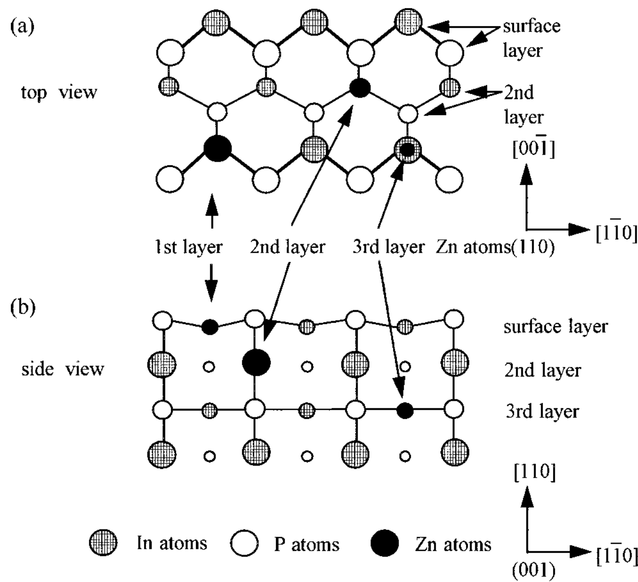

FIG. 5. Schematic explanation of the symmetry of the substitional Zn_{In} atoms in different subsurface layers.

atoms are located along the [1$\bar{1}$0] rows. In addition, the P atoms in the [001] direction are always a little bit closer to the Zn atom, and thus should be raised higher than those in the [00$\bar{1}$] direction. This is due to the fact that the Zn atom is displaced by $\frac{1}{4}a$ in the [001] direction. This situation described here is that observed for defect *a* in Fig. 2.

In contrast, the Zn atom in the second layer has only one closest-neighbor P atom in the surface layer. Furthermore, the Zn atom is also displaced by $\frac{1}{4}a$, but in the (opposite) [00$\bar{1}$] direction compared to the Zn atom in the surface layer. Since the Zn is located further away from the surface the band bending on the surface and consequently the elevation in STM images is smaller compared to that of a Zn atom in the surface layer. This configuration is reflected by the Zn-dopant atom in Fig. 2(b).

Finally, the Zn in the third layer again has the same symmetry as that in the surface layer. It induces only a smaller band bending on the surface because of its larger depth. The dopant atom in Fig. 2(c) belongs to this subsurface layer.

Up to now we have only considered substitutional Zn_{In} atoms. Zn_P on P lattice sites can be excluded, since Zn is known to be either on In or interstitial sites. Furthermore the symmetry/brightness relation does not agree with P lattice sites. Zn_i on interstitial sites can also be excluded, because it is expected to be positively charged in InP (Ref. 24) and would also have a different symmetry behavior. In addition, it is conceivable that Zn on near-surface interstitial sites will relax after cleavage onto the surface, and probably evaporate due to the low vapor pressure.

Thus it can be concluded that substitutionally incorporated Zn-dopant atoms can be observed and distinguished in three different subsurface layers. In fact the dopant atoms can be observed depending on the quality of the tip up to six layers deep (about one screening length deep). The broad-band bending in our samples makes it difficult, however, to observe the symmetries of dopants in such deep layers reliably, because the noise level obscures the decreasing relative height changes from atom to atom.

D. Comparison with observations of Zn and Be dopants in GaAs(110)

The Zn-dopant atoms observed on InP(110) have many similarities to those observed on GaAs(110) surfaces.[7–9] On both surfaces the dopant atoms are negatively charged and have the same symmetry alternating with even and odd subsurface layers. The dopants can be observed in both cases up to about six subsurface layers deep. No lattice relaxations are observable around the dopant atoms in both materials, although the Zn substitutes (ion radius 0.083 nm) a larger In ion (0.092 nm) in InP, and a smaller Ga ion (0.062 nm) in GaAs. Thus the contrast visible in STM images is only induced by the charge accumulation around the negative charge. Be dopant atoms[7] in GaAs show the same features. For a Si_{Ga} donor in the GaAs(110) surface layer, a well-localized charge has been predicted.[25] This gives a specific signature to the Si donors, which has not been observed for the Zn or Be acceptors.[7,8] The acceptors have no localized state in the STM images.

IV. VACANCY-DOPANT COMPLEXES AND DIPOLES

A. Structure and appearance of vacancy-dopant complexes and dipoles

In Sec. III we studied only isolated Zn-dopant atoms. However, if the vacancy concentration increases, the probability of finding a close vacancy-Zn pair is raised, and defects like that labeled *V*/Zn in Fig. 1 can be observed with increasing density. Figures 6(a) and 6(b) show high-resolution images of two different types of such defects. For comparison a positively charged vacancy far away from any Zn dopant is displayed in Fig. 6(c). The defects in Figs. 6(a) and 6(b) are not surrounded by any height changes (elevation or depression) like those around dopants and vacancies. Thus they do not induce a band bending and are uncharged overall. They always consist of one localized hole of the size of one phosphorus dangling bond, and one or two apparently raised dangling bonds. Figures 6(d)–6(f) show a series of vacancies at different distances from Zn-dopant atoms. Zn-vacancy pairs with a large separation do not change each others' appearance and properties. However, as the separation is reduced, both the vacancy and the Zn have a less pronounced band bending [compare the two dopant atoms in Fig. 6(d)]. Finally, if the Zn is a direct neighbor of the vacancy, defect complexes like those in Figs. 6(a) and 6(b) are formed. Figures 6(d)–6(f) are still separate defects and thus atomic scale dipoles.

The origin of the defects can be confirmed by analyzing the height profiles through them (Fig. 7).[13] The profiles are comparable, since they were obtained with the same tip state, set current, and tunneling voltage. Profiles *a* and *b* show height changes induced by an isolated negatively charged Zn-dopant atom and an isolated positively charged phosphorus vacancy. As discussed above, the height change of the Zn atom is mostly due to the charge accumulation around the negatively charged ion. If the two profiles *a* and *b* are added (*a* without the atomic corrugation in order to add only the

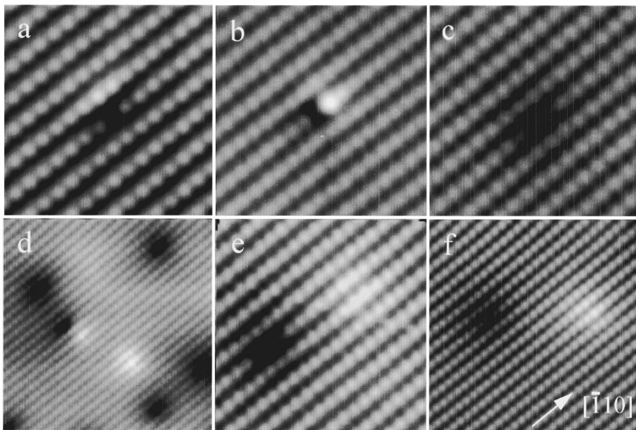

FIG. 6. Vacancy-Zn defect complexes and dipoles. (a) and (b) show two complexes, (c) an isolated vacancy for comparison, and (d)–(f) dipoles with different separations. The images have the same orientation as those in Fig. 1.

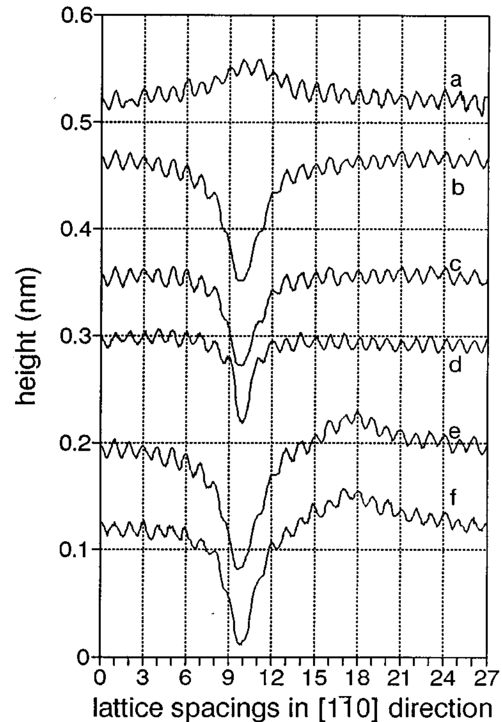

FIG. 7. Height profiles through (curve a) a negatively Zn-dopant atom, (curve b) a positively charged P vacancy, (curve c) the sum of a and b showing the structural relaxation of the vacancy, (curve d) a charge-compensated vacancy (defect complex), (curve e) the sum of a and b offset by seven lattice spacings, and (curve f) the profile of a dipole consisting of a vacancy and a Zn atom separated by seven lattice spacings. All linecuts have been measured with the same tip at -2.1 V and 0.8 nA. The profiles were measured along the $[\bar{1}10]$ direction (along the apparent atomic rows).

height change induced by the charge accumulation), the depletion zone around the vacancy is compensated by the accumulation zone around the Zn and the resulting profile should only show the structural relaxations of the vacancy (profile c). For comparison a profile (d) has been obtained for a vacancy dopant complex like that displayed in Fig. 6(a). It matches well with the calculated profile (c), suggesting that the defect in Fig. 6(a) is in fact a (partially) charge-compensated Zn-vacancy defect complex. If the dopant atom is displaced relative to the vacancy by seven lattice spacings in the $[1\bar{1}0]$ direction, the sum of profiles a and b yields profile e. The latter can be compared with a measured profile of the vacancy-Zn dipole in Fig. 6(e) (profile f). Again they agree well. It should be noted that profiles c and d are not completely charge compensated, since the Zn-dopant atom is in a subsurface layer.

The defect complexes in Figs. 6(a) and 6(b) are nearly completely compensated. However, the voltage dependence in Fig. 8 reveals that there is still a very small charge accumulation and depletion at the site of the Zn and the vacancy, respectively. For example, if the magnitude of the voltage decreases, the neighboring dangling bond(s) in Figs. 8(c) and 8(f) both appear brighter, while the dangling bonds on the other side of the vacancy appear darker. Thus even the defect complexes are still atomic scale dipoles. This effect is small and only observable at very low negative tunneling voltages, but it allows us to deduce the most likely location of the Zn atom relative to the vacancy: the Zn atom in Figs. 8(a)–8(c) is localized in the second layer, as indicated by its mirror symmetry on top of a [001] row. Furthermore it has its maximum in the neighboring $[1\bar{1}0]$ row compared to the vacancy. The Zn atom in Figs. 8(c)–8(f) is a nearest neighbor of the vacancy in the $[1\bar{1}0]$ direction. We observed Zn on all In sites around the vacancies with roughly the same frequency.

B. Charge compensation of dipoles and the vacancy charge

The charge compensation of vacancies and Zn-dopant atoms can be analyzed better after the subtraction of all structural contributions to the STM images. We will demonstrate this for the dipole in Fig. 6(e) using the profiles of Fig. 7. Profile f in Fig. 7 is a composite of both the charge accumulation and depletion and the structural relaxation around the vacancy (including the missing dangling bond). The latter can be estimated from profiles c and d in Fig. 7, which just show the structural properties of the vacancy (with no charge). Thus subtracting the structural properties of the vacancy (profile d) from the dipole profile f yields in sufficient approximation the height change induced by the charge-carrier accumulation and depletion [Fig. 9].

Figure 9 shows that the vacancy-Zn combination is in fact a dipole. For comparison the respective height changes induced by the charge-carrier clouds of the isolated Zn and vacancy have been included in Fig. 9. Both isolated defects have a larger height change (in magnitude and extension) than the respective areas of the dipole. This indicates that the Zn and vacancy charges are indeed partly compensated. The degree of compensation can be estimated by comparing the integral of the profiles. It is found that the integrals of the dipole charge accumulation and depletion are about 70% of those of the isolated Zn and vacancy, respectively. Although this is not proportional to the real charge accumulated, it gives a rough estimate of the charge compensation. For the calculation of the real charge accumulation it is necessary to take into account that the charge cloud is noncylindrical and three dimensional.

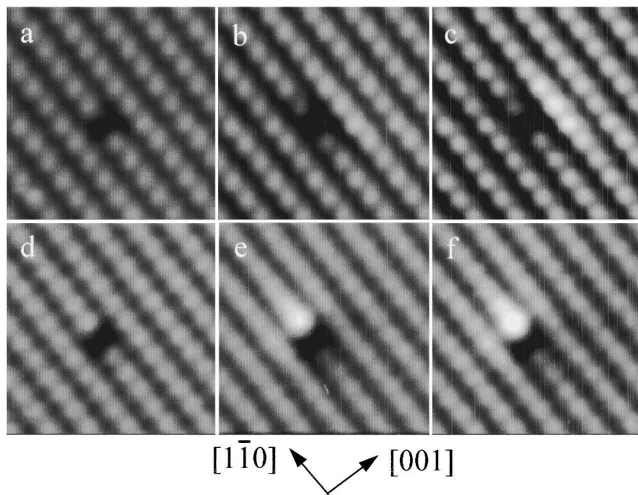

FIG. 8. Voltage dependence of the defect complexes in Figs. 6(a) and 6(b). The images were measured at (a) −3.3, (b) −2.1, (c) −1.4, (d) −3.3, (e) −2.0, and (f) −1.5 V.

Figure 10 shows the estimations of the degree of charge compensation as a function of the separation of the vacancy-Zn pairs. It indicates a gradual charge compensation with decreasing separation. This gradual change suggests that the vacancy and the Zn can completely compensate each other if they reach the same lattice site. This agrees with the observation of no-long-range charge screening or band bending around the Zn-vacancy defect complexes. Thus the total charge of the complexes is 0. Only a dipole field is left. If one assumes that a near-surface Zn-dopant atom has a charge of $-1e$ as in the bulk,[24] the vacancy must have a $+1e$ charge. This result agrees with an independent previous charge determination of the vacancies on InP(110),[23] and with a similar compensation that has been observed for As vacancies on GaAs(110).[13]

C. Interactions between dopants and vacancies

Defects can interact with each other. If this interaction is repulsive, the defects try to avoid each other and defect complexes are energetically unfavorable. However, an attractive interaction can result in a considerable increase of the concentration of defect complexes, since the defect complex may be energetically more favorable than single defects. Information about an attractive or repulsive interaction can be deduced from the occurrence of pairs as a function of their separation. If this pair distribution function is divided by that of randomly distributed noninteracting pairs, the pair-correlation function is obtained.[26] Figure 11 shows the pair-correlation function of vacancy-Zn pairs as a function of the pair separation *projected on the surface*. The correlation function shows a strong increase for distances shorter than about 1.5 nm, indicating an attractive interaction. The fact that the vacancies and dopants have opposite charges makes an attraction conceivable.

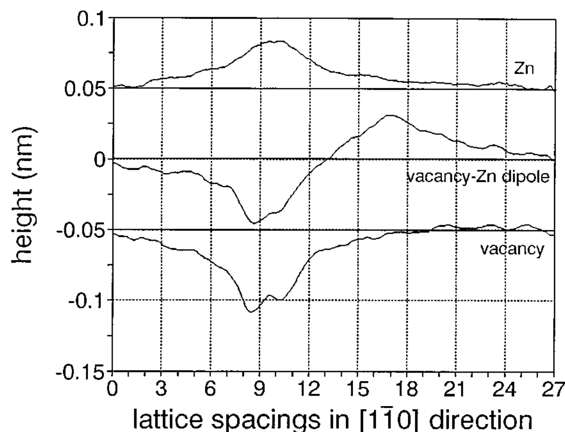

FIG. 9. Height change due to the charge accumulation and depletion of a vacancy, a vacancy-Zn dipole, and a Zn dopant. The data have been obtained from the linecuts (a), (b), and (f) in Fig. 7.

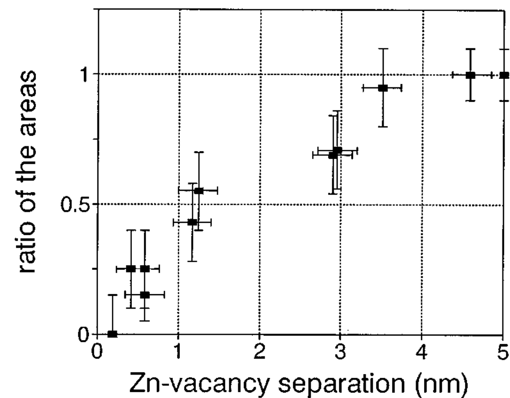

FIG. 10. Relative surface area in Fig. 9 of the dipole for different vacancy-Zn separations. The data can be understood with a gradual compensation of the charge accumulation and depletion zones around the vacancies.

It should be noted that the determination of the pair distribution function for noninteracting pairs is difficult because of the low number of pairs observed at greater distances (due to the attraction). Therefore we calculated the theoretical pair distribution function using the measured vacancy and dopant concentrations. We assumed that dopants in the first three or four subsurface layers may attract surface vacancies. This results in the pair-correlation function in Fig. 11. If the Zn atoms in the deeper subsurface layer also influence the vacancies, the hole correlation function may be shifted slightly downward (logarithmic scale), but the strong increase below 1 nm separation is not affected.

D. Concentration of electrically active dopants: Influence of vacancies

Figure 12 shows two images obtained after annealing the samples at 480 K for 5 and 1100 min. Two features can be observed: the concentration of vacancies increases and the concentration of negatively charged Zn-dopant atoms decreases. In Fig. 12(a) eight Zn_{In}^- can be observed, while in Fig. 12(b) only one is left. We purposely chose a STM image with an observable dopant atom for Fig. 12(b) in order to demonstrate that the reduction is not due to imaging conditions of the tip, allowing no observation of dopants. For most images no dopant atoms were found at all.

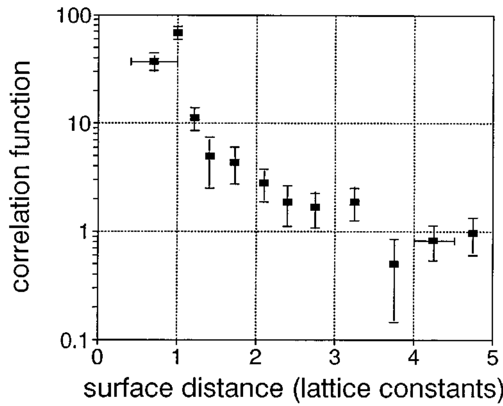

FIG. 11. Pair-correlation function between vacancies and Zn atoms as a function of their projected separation on the surface.

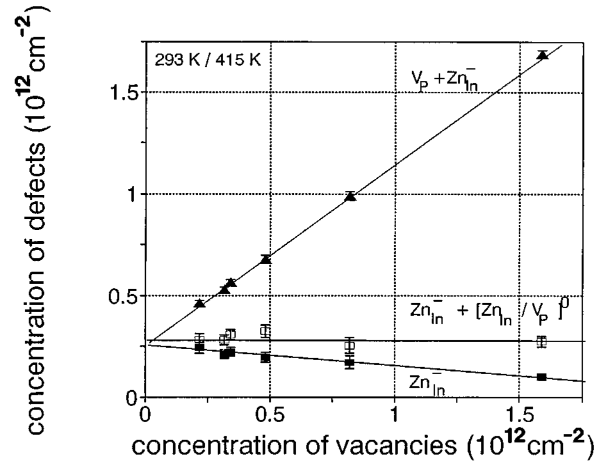

FIG. 13. Concentration of the electrically active Zn dopants (Zn_{In}^-), of the uncharged Zn-vacancy defect complexes and electrically active Zn dopants ($[V_P/Zn_{In}]^0+Zn_{In}^-$) (total observable Zn concentration), and of the vacancies and electrically active Zn dopants ($V_{P+}+Zn_{In}^-$) as a function of the vacancy concentration. The data have been obtained on samples annealed at 293 and 415 K.

At low temperatures (293 and 415 K) the decrease of the charged dopant atoms is proportional to the vacancy concentration (Fig. 13). At the same time the concentration of Zn-vacancy complexes increases, also proportionally to the vacancy concentration. The sum of the observable isolated charged Zn atoms and the defect complexes, however, remains constant with the vacancy concentration and time (Fig. 13).

This observation of the decrease of electrically active Zn atoms can be explained by the probability of finding a vacancy close to a dopant atom. If the vacancy concentration increases, the complexes formed must increase proportionally, and the remaining charged Zn atoms become fewer. As long as no vacancy leaves the surface plane and no Zn atom desorbs or migrates, the total concentration of Zn is thus the sum of the densities of defect complexes and charged Zn atoms. The total concentration of Zn should remain constant, as observed. This interpretation also implies that all vacancy-Zn complexes formed have their vacancy in the surface layer, while the Zn atom may be in some subsurface layers. Thus on the surface the average dipoles have their positive charge on the surface, while the negative charge is at or below the surface.

It should be noted that most charged Zn atoms visible at high vacancy concentration are Zn atoms several subsurface layers deep in the crystal. They have a smaller attraction on surface vacancies and thus remain isolated for the longest time. Essentially no isolated surface Zn atom was observed for higher vacancy concentrations.

In Fig. 13 the slope of the Zn_{In}^- concentration as a function of the vacancy density is -0.1. This value shows that about 10% of the vacancies are compensated by (or compensate) a Zn atom. If there were no interaction between the vacancies and dopant atoms this value should be about 6% for a complete compensation by Zn atoms in the first six subsurface layers (using the measured concentration). The observed higher compensation rate also corroborates the existence of an attractive interaction between the vacancies and dopant atoms.

The sum of the vacancy concentration and charged Zn concentration in Fig. 13 is not constant. This situation is unlike that in a previous study on GaAs with samples having a ten-times-higher Zn-dopant concentration.[13] There about 80% of the vacancies are compensated. The higher Zn concentration is the reason for this different behavior: at high-Zn concentrations nearly every vacancy has a Zn atom close

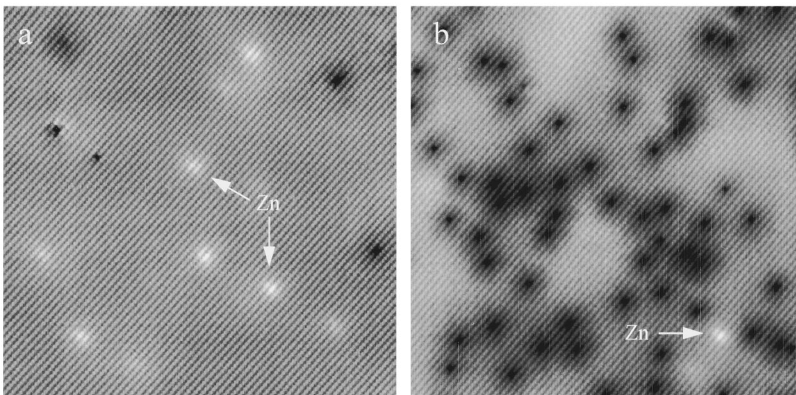

FIG. 12. Reduction of the concentration of negatively charged dopant atoms with increasing vacancy concentration. (a) has been measured after 5 min and (b) after about 1100-min annealing at 480 K. In the lower right corner of (b) a dopant atom is visible, showing that the dopant atoms can be in principle observed. The images have the same orientation as those in Fig. 1.

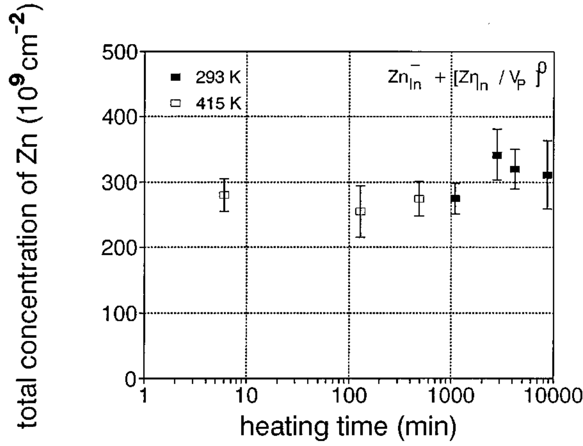

FIG. 14. Concentration of the total observable Zn concentration ($[V_P/Zn_{In}]^0+Zn_{In}^-$) as a function of the time at 293 and 415 K.

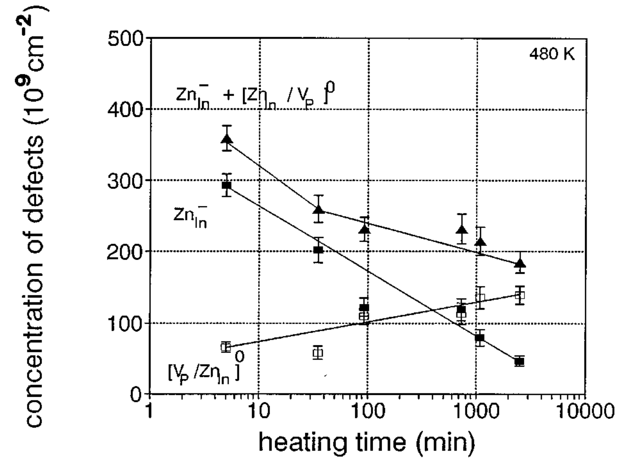

FIG. 15. Concentration of the Zn_{In}^-, $[V_P/Zn_{In}]^0$, and $[V_P/Zn_{In}]^0+Zn_{In}^-$ as a function of time at 480 K.

enough to compensate each other. Thus as the vacancy concentration increases the Zn concentration decreases nearly equally.

V. TEMPERATURE AND TIME DEPENDENCE OF THE DOPANT CONCENTRATION

A. Decrease of the observable Zn atoms in the surface at high temperatures

Up to now we have only studied the concentration of charged dopant atoms and defect complexes as a function of the vacancy concentration. However, the vacancy concentration is not an independent variable, since the formation of vacancies is governed by the annealing *time* and *temperature*. Thus the real independent variables are time and temperature. The statistical analysis performed in Sec. IV D has been done for low temperature in the range of 293–415 K. In this range the total concentration of observable Zn atoms in the surface layers (sum of the charged Zn and uncharged vacancy-Zn complexes) remains unchanged with the heating time (Fig. 14), allowing us to perform the previous analysis. We would like to mention that the doping concentrations in Fig. 14 vary slightly between the two samples because of inhomogeneities of the Zn concentration in the wafer used.[14] The relative differences in Zn concentration on one sample can, however, be reliably measured with STM.

In contrast to the measurements at low temperatures (<415 K) the observable Zn concentration in the surface is decreasing with time by a factor of about 2 after 2500 min of annealing at 480 K. As for low temperatures, the density of negatively charged Zn atoms decreases, but the increase of the concentration of defect complexes (with a vacancy in the surface layer) does not compensate for the loss of charged isolated Zn atoms.

B. Discussion of possible mechanisms reducing the observable Zn concentration

There are several possible mechanisms which can lower the observable Zn concentration at higher temperatures (see Fig. 15). For the following discussion it should be kept in mind that STM does not necessarily allow us to measure the total concentration of Zn in the surface and the first few subsurface layers. In particular we cannot observe uncharged defects or defect complexes below the surface layer.

We will discuss the following mechanisms: (i) Formation of compensating defect complexes in subsurface layers (with immobile Zn). (ii) Real depletion of the Zn concentration in the surface by Zn diffusion.

In the following we will present arguments leading to the conclusion that the apparent Zn depletion is due to the formation of uncharged subsurface defect complexes. If such defect complexes are uncharged, no band bending can be observed on the surface. Since we can only observe subsurface Zn atoms due to their charge-induced band bending, each uncharged subsurface defect complex thus formed will reduce by one the number of observable Zn atoms, even if the Zn atoms remain immobile. In order to compensate a dopant atom in the bulk, a $+1e$ charged bulk defect must be introduced into the subsurface layers. If the defect has another charge, the complex will not be completely compensated, and will have a remaining positive or negative charge. In the latter case we would detect it on the surface. However, we did not observe positive subsurface charges in the necessary concentration (negative charges would have been counted as one dopant atom). Thus the defect complexes must be uncharged (similarly to those on the surface), and thus the defect introduced in the bulk $+1e$ is charged.

At this stage one can ask what kind of defect can compensate the dopants. This compensating defect must be $+1e$ charged. Simultaneously one should take into account that a previous study of the thermal formation of vacancies revealed that the vacancy formation rate increases up to 435 K. Above that temperature it decreases. This observation adequately matches the temperature dependence of the decrease of the effective Zn concentration. The decrease of the vacancy formation rate had been explained by outdiffusion of phosphorus from the bulk, while the exact atomistic process remained undetected,[12] but this may nevertheless give some indication of which defects can compensate the Zn dopants.

The outdiffusion of phosphorus can occur via two atomic processes, the interstitial diffusion of P to the surface and the migration of vacancies into the bulk (substitutional diffusion). In our case this would result in $[P_i/Zn_{In}]$ and $[V_P/Zn_{In}]$ defect complexes, respectively. We now use theoretical calculations to find out which of these defect complexes can be uncharged. A charge of $+3e$ is predicted for the interstitial anions in p-type InP,[24] GaAs,[27] and GaP,[27] while a charge of $+1e$ is predicted for an anion vacancy in the respective anion-rich materials.[24,27–31] In addition, the As vacancy in the GaAs bulk was found to be a simple donor.[32] This suggests that only the formation of subsurface phosphorus-vacancy–Zn-dopant atom complexes can explain the decrease of the observable Zn concentration. For completeness we can also exclude other defects, such as antisites, In interstitials, or In vacancies, as the compensating defect, because they do not have a single positive charge.[24] They could only act as compensation if they compensated several close Zn atoms simultaneously. This, however, appears unlikely at our dopant concentration.

This explanation does not exclude, however, that interstitial diffusion of phosphorus also reduces the vacancy formation rate. The latter mechanism may be responsible for the strong decrease of the vacancy concentration at 575 K, and may destroy all vacancy-Zn complexes formed by filling the vacancies and thus making the Zn atoms observable. It could also be that at this temperature the vacancies are sufficiently mobile to leave the Zn atoms and diffuse freely into the crystal. At the present stage this matter cannot be resolved.

For the formation of subsurface vacancy-Zn complexes the vacancies need a certain mobility. The vacancies have enough mobility to migrate on the surface, but migration into the subsurface layers requires a higher energy (similar to that for diffusion in the bulk). Radioactive tracer experiments on bulk InP yielded an activation energy for bulk diffusion of 5.65 eV.[33] This would exclude substitutional P from playing any role in the temperature range investigated in our experiments. However, the results in the literature are contradictory,[34] since results of emission channeling[35] and electron paramagnetic resonance experiments[36] suggest that vacancies may be mobile at 400 K. Even if the vacancies cannot yet migrate at those temperatures in the bulk, there are two reasons why they may nevertheless migrate toward the subsurface Zn atoms: First, it is conceivable that the diffusion energies for the first few subsurface layers may be significantly different from the bulk. Second, the Zn atoms are negatively charged, and the attractive interaction potential between them and a positively charged vacancy may lower the migration barrier toward the Zn atom (but not away from it or at a place without Zn atoms). Thus the positive vacancies may be attracted a few layers into the surface and form immobile complexes.

A real surface depletion of Zn can be excluded, since it is well known that the diffusion of substitutionally incorporated Zn atoms occurs only at very high temperatures. For example, in GaAs and InP this seems to start at about 1000 K.[37,38] Our measurements, however, were performed below 480 K. If, nevertheless, such an outdiffusion of Zn were to occur, this mechanism should be even faster at even higher temperatures. However, at 575 K we again observed a normal surface concentration of Zn. At this high temperature the concentration of vacancies is very low. This reduces the probability of vacancy-Zn complexes and again confirms that defect complexes play a role in the decrease of the observable Zn concentration. A surface depletion due to Zn migration into the crystal can also be excluded, because the diffusion would increase the concentration gradient. Furthermore the solubility of Zn on substitutional lattice sites in InP is limited and lower than in GaAs. Since our crystals are already relatively highly doped, Zn migration into the crystal is implausible.

VI. SUMMARY

We presented a comprehensive study of Zn-dopant atoms and their surface and subsurface defect complexes on InP (110). Electrically active Zn atoms in different subsurface layers can be distinguished by their symmetry and effective charge accumulation on the surface. These isolated electrically active Zn atoms can be compensated by vacancies forming defect complexes with atomic scale dipoles. The formation of vacancy-Zn complexes has been investigated as a function of the vacancy density, annealing time, and temperature. It is found that the observable Zn concentration remains constant in a low-temperature range (up to 415 K) but decreases at 480 K. This is explained by the formation of defect complexes consisting at low temperatures of a *surface* vacancy and a subsurface or surface Zn atom, while at higher temperatures uncharged subsurface defect complexes are formed. It is proposed that these consist of a *subsurface* vacancy and a Zn atom.

ACKNOWLEDGMENTS

The authors would like to express their thanks to Zhenyu Zhang for helpful discussions, and to K. H. Graf for technical support. Ph.E. thanks the Alexander von Humboldt-Foundation for support.

[1] M. B. Johnson, P. M. Koenraad, W. C. van der Vleuten, H. W. M. Salemink, and J. H. Wolter, Phys. Rev. Lett. **75**, 1606 (1995).

[2] A. García and J. E. Northrup, Phys. Rev. Lett. **74**, 1131 (1995).

[3] R. M. Feenstra, J. M. Woodall, and G. D. Petit, Phys. Rev. Lett. **71**, 1176 (1993).

[4] Ph. Ebert and K. Urban, Ultramicroscopy **49**, 344 (1993).

[5] G. Lengel, R. Wilkins, G. Brown, M. Weimer, J. Gryko, and R. E. Allen, Phys. Rev. Lett. **72**, 836 (1994).

[6] Ph. Ebert, K. Urban, and M. G. Lagally, Phys. Rev. Lett. **72**, 840 (1994).

[7] M. B. Johnson, O. Albrektsen, R. M. Feenstra, and H. W. M. Salemink, Appl. Phys. Lett. **63**, 2923 (1993); **64**, 1454 (1994).

[8] J. F. Zheng, M. B. Salmeron, and E. R. Weber, Appl. Phys. Lett. **64**, 1836 (1994); **65**, 790 (1994).

[9] M. Simon, C. Dzeja, Ph. Ebert, H. G. Hettger, W. Jäger, A. Rucki, and K. Urban, in *Proceedings of the 4th International Confer-*

ence on the Formation of Semiconductor Interfaces, Jülich, 1993, edited by B. Lengeler, H. Lüth, W. Mönch, and J. Pollmann (World Scientific, Singapore, 1994), p. 49.

[10] J. F. Zheng, X. Liu, E. R. Weber, D. F. Ogletree, and M. Salmeron, J. Vac. Sci. Technol. A **12**, 2104 (1994)

[11] J. F. Zheng, X. Liu, N. Newman, E. R. Weber, D. F. Ogletree, and M. Salmeron, Phys. Rev. Lett. **72**, 1490 (1994)

[12] Ph. Ebert, M. Heinrich, M. Simon, K. Urban, and M. G. Lagally, Phys. Rev. B **51**, 9696 (1995).

[13] K.-J. Chao, A. R. Smith, and C. K. Shih, Phys. Rev. B (to be published).

[14] A high sensitivity chemical analysis showed a slight variation of the Zn concentration of about $(1.7–3)\times10^{18}$ cm^{-3} within the wafer. The variation observed by STM is, however, much smaller.

[15] K. Besocke, Surf. Sci. **181**, 145 (1987).

[16] Ph. Ebert, G. Cox, U. Poppe, and K. Urban, Ultramicroscopy **42-44**, 871 (1992).

[17] M. Heinrich, Ph. Ebert, M. Simon, K. Urban, and M. G. Lagally, J. Vac. Sci. Technol. A **13**, 1714 (1995).

[18] G. Cox, Ph. Ebert, and K. Urban, in *Microscopy of Semiconducting Materials,* edited by A. G. Cullis and N. J. Long, IOP Conf. Proc. No. 117 (Institute of Physics, Bristol, 1991), p. 347.

[19] M. B. Johnson, H. P. Meier, and H. W. M. Salemink, Appl. Phys. Lett. **63**, 3636 (1993).

[20] R. J. Hamers, J. Vac. Sci. Technol. B **6**, 1462 (1988).

[21] J. A. Stroscio, R. M. Feenstra, and A. P. Fein, Phys. Rev. Lett. **58**, 1668 (1987).

[22] G. Lengel, R. Wilkins, G. Brown, and M. Weimer, J. Vac. Sci. Technol. B **11**, 1472 (1993).

[23] Ph. Ebert, Xun Chen, M. Heinrich, M. Simon, K. Urban, and M. G. Lagally, Phys. Rev. Lett. (to be published).

[24] R. W. Jansen, Phys. Rev. B **41**, 7666 (1990).

[25] J. Wang, T. A. Arias, J. D. Joannopoulis, G. W. Turner, and O. L. Alerhand, Phys. Rev. B **47**, 10 329 (1993).

[26] T. L. Hill, *Statistical Mechanics* (McGraw-Hill, New York, 1956).

[27] R. W. Jansen and O. F. Sankey, Phys. Rev. B **39**, 3192 (1989).

[28] G. A. Baraff and M. Schlüter, Phys. Rev. Lett. **55**, 1327 (1985).

[29] M. Alatalo, R. M. Nieminen, M. J. Puska, A. P. Seitsonen, and R. Virkkunen, Phys. Rev. B **47**, 6381 (1993).

[30] A. P. Seitsonen, R. Virkkunen, M. J. Puska, and R. M. Nieminen, Phys. Rev. B **49**, 5253 (1994).

[31] J. E. Northrup and S. B. Zhang, Phys. Rev. B **50**, 4962 (1994).

[32] S. Y. Chiang and G. L. Pearson, J. Appl. Phys. **46**, 2986 (1975).

[33] B. Goldstein, Phys. Rev. **121**, 1305 (1961).

[34] K. Karsten (unpublished).

[35] U. Wahl, H. Hofsäss, S. G. Jahn, S. Winter, and E. Recknagel, Nucl. Instrum. Methods Phys. Res. Sect. B **64**, 221 (1992).

[36] H. J. Bardeleben, Solid State Commun. **57**, 137 (1986).

[37] S. Yu, T. Y. Tan, and U. Gösele, J. Appl. Phys. **69**, 3547 (1991).

[38] Tan Litong, Zhou Junglong, and Fang Dunfu, Mater. Sci. Forum **61**, 29 (1990).